JOURNAL OF THE ROYAL SOCIETY Interface

Towards optimization of patterned superhydrophobic surfaces

Bharat Bhushan, Michael Nosonovsky and Yong Chae Jung

J. R. Soc. Interface 2007 **4**, 643-648
doi: 10.1098/rsif.2006.0211

JOURNAL OF THE ROYAL SOCIETY Interface

J. R. Soc. Interface (2007) **4**, 643–648
doi:10.1098/rsif.2006.0211
Published online 23 January 2007

Towards optimization of patterned superhydrophobic surfaces

Bharat Bhushan[1,*], Michael Nosonovsky[2] and Yong Chae Jung[1]

[1]*Nanotribology Laboratory for Information Storage and MEMS/NEMS (NLIM), The Ohio State University, 201 West 19th Avenue, Columbus, OH 43210-1142, USA*
[2]*National Institute of Standards and Technology, Gaithersburg, MD 20899-8520, USA*

Experimental and theoretical study of wetting properties of patterned Si surfaces with cylindrical flat-top pillars of various sizes and pitch distances is presented. The values of the contact angle (CA), contact angle hysteresis (CAH) and tilt angle (TA) are measured and compared with the theoretical values. Transition from the composite solid–liquid–air to the homogeneous solid–liquid interface is investigated. It is found that the wetting behaviour of a patterned hydrophobic surface depends upon a simple non-dimensional parameter, the spacing factor, equal to the pillar diameter divided by the pitch. The spacing factor controls the CA, CAH and TA in the composite interface regime, as well as destabilization and transition to the homogeneous interface. We show that the assumption that the CAH is a consequence of the adhesion hysteresis and surface roughness leads to the theoretical values of the CAH that are in a reasonably good agreement with the experimental values. By decreasing the spacing factor, the values of CA = 170°, CAH = 5° and TA = 3° are achieved. However, with further decreasing of the spacing factor, the composite interface destabilizes.

Keywords: hydrophobic; lotus effect; contact angle; hysteresis; tilt angle

1. INTRODUCTION

The advances in nanotechnology, including micro/nanoelectromechanical systems, have stimulated the development of new materials and design of surfaces that should be water-repellent or hydrophobic. Wettability is characterized by the static contact angle (CA) between a water droplet and a surface. A surface is hydrophilic if the value of the CA is less than 90°, whereas the surface is hydrophobic if the value of the CA is greater than 90°. Surfaces with CA between 150° and 180° are called superhydrophobic. The CA depends on several factors, such as surface energy, roughness, the manner of surface preparation and surface cleanliness (Adamson 1990; Israelachvili 1992; Bhushan 1999, 2002, 2005, 2007).

Superhydrophobic surfaces have very low water contact angle hysteresis (CAH), defined as the difference between the advancing and receding CA. If liquid is added to a sessile drop, the contact line advances and an advancing CA is measured. Alternatively, if liquid is removed from the drop, the CA decreases to a receding value before the contact retreats. For a droplet moving along the solid surface, the CA at the front of the droplet (advancing CA) is greater than that at the back of the droplet (receding CA), due to roughness and surface heterogeneity, resulting in the CAH. Physical reasons for the CAH are still debated in the literature, but surface roughness and inhomogeneity are believed to be responsible for the almost universal occurrence of the CAH (Israelachvili 1992). In addition to high CA and low CAH, another wetting property of interest for liquid flow applications is a very low water roll-off angle or tilt angle (TA), which denotes the angle to which a surface may be tilted for roll off of water droplets (Extrand 2002, 2006; Kijlstra *et al.* 2002).

In the past decade, many researchers have studied hydrophobic surfaces that are found in nature. Among them are the leaves of water-repellent plants such as *Nelumbo nucifera* (lotus) and *Colocasia esculenta*, which have a high CA with water and show strong self-cleaning properties known as the 'lotus effect' (Barthlott & Neinhuis 1997; Wagner *et al.* 2003). These leaf surfaces are covered with microbumps (called *papillae*), which, in turn, are covered with hydrophobic wax with nanoscale roughness (Burton & Bhushan 2006; Bhushan & Jung 2006). Extensive research of hydrophobic plant waxes has been conducted by plant scientists and lipid chemists in the past decades (Jetter *et al.* 2006). For the lotus leaf, the combination of wax and bumps leads to a high value of CA of 162° (Neinhuis & Barthlott 1997). A number of studies have been carried out to produce artificial biomimetic roughness-induced hydrophobic surfaces (Shibuichi *et al.* 1996; Hozumi & Takai 1998; Coulson *et al.* 2000; Miwa *et al.* 2000; Oner & McCarthy 2000; Feng *et al.* 2002; Erbil *et al.* 2003; Lau *et al.* 2003; Burton & Bhushan 2005; Li & Amirfazli 2005; Jung & Bhushan 2006). Hydrophobic surfaces can be designed by using low surface energy materials or coatings, such as polytetrafluoroethylene or wax. The hydrophobicity of a surface can also be increased by surface roughness and/or creation of air pockets. Air may be trapped in the cavities

*Author for correspondence (bhushan.2@osu.edu).

Received 6 December 2006
Accepted 30 December 2006

of a rough surface, resulting in a composite solid–air–liquid interface, as opposed to the homogeneous solid–liquid interface (Wenzel 1936; Cassie & Baxter 1944; Johnson & Dettre 1964; Nosonovsky & Bhushan 2005, 2006). Recent studies have investigated the stability of the composite interface of artificial superhydrophobic surfaces and transition from the composite to homogeneous interface (the opposite transition has never been observed). Several researchers also paid attention to the importance of the multiscale roughness for the superhydrophobicity (Lafuma & Quéré 2003; Gao & McCarthy 2006). Nosonovsky & Bhushan (in press) suggested that destabilizing factors responsible for such a transition have different characteristic scale lengths, and thus multiscale roughness plays an important role in stabilizing the composite interface. Based on modelling and experiments, it has been shown that whether the interface is solid–liquid–air composite or solid–liquid homogeneous may depend on several factors, such as the roughness distribution of the surface, levels of energy corresponding to the composite and homogeneous interfaces, history of formation of the droplet, magnitude of gravity and surface forces, effect of contact line continuity or contact line density, etc. (Chen *et al.* 1999; Bico *et al.* 2002; Marmur 2003; Lafuma & Quéré 2003; Patankar 2003; He *et al.* 2003; Fürstner *et al.* 2005; Extrand 2002, 2006).

In this paper, we present a study of patterned Si surfaces with cylindrical pillars of different diameters, heights and pitch distance in order to investigate the dependence of the CA, CAH and TA upon the geometrical parameters. We identify a simple non-dimensional geometrical parameter, which is responsible for the wetting properties. The experimental data are compared with the theoretical calculation, and this allows us to derive conclusions about the physical mechanisms responsible for the CAH and those leading to the destabilization of the composite interface.

2. THEORETICAL CALCULATION OF CONTACT ANGLE, CONTACT ANGLE HYSTERESIS AND TILT ANGLE

Young's equation (Adamson 1990; Israelachvili 1992) relates the static CA of a droplet in equilibrium upon a smooth surface, θ_0, to the free surface energies of the solid–liquid, solid–air and liquid–air interfaces, γ_{SL}, γ_{SA} and γ_{LA}, respectively,

$$\cos\theta_0 = \frac{\gamma_{SA} - \gamma_{SL}}{\gamma_{LA}}. \tag{2.1}$$

For a droplet in contact with a rough surface without air pockets, the CA, θ, is given by the Wenzel (1936) equation

$$\cos\theta = R_f \cos\theta_0, \tag{2.2}$$

where R_f is a roughness factor defined as

$$R_f = \frac{A_{SL}}{A_F}, \tag{2.3}$$

where A_F is the flat solid–liquid contact area or a projection of the solid–liquid area A_{SL} on the horizontal plane. For a composite interface with air pockets having fractional solid–liquid contact area f_{SL}, the CA is given by the Cassie & Baxter (1944) equation

$$\cos\theta = R_f f_{SL} \cos\theta_0 - 1 + f_{SL}. \tag{2.4}$$

When liquid comes in contact with a solid, the solid–liquid interface is created while solid–air and liquid–air interfaces are destroyed. The work of adhesion between the liquid and the solid per unit area is therefore given by the Dupré equation (Adamson 1990)

$$W = \gamma_{SA} + \gamma_{LA} - \gamma_{SL} = \gamma_{LA}(1 + \cos\theta). \tag{2.5}$$

It is well known that the energy gained for surfaces that come into contact is greater than the work of adhesion for separating the surfaces by the quantity ΔW, due to the so-called adhesion hysteresis (Ruths *et al.* 2005). The adhesion hysteresis is related to the CAH, although it does not uniquely define the latter. There are many factors that affect the CAH, including the adhesion hysteresis, surface roughness and heterogeneity. For an exact theoretical calculation of the CAH, a thermodynamic analysis of energy barriers for a moving droplet would be required (Johnson & Dettre 1964; Wolansky & Marmur 1998; Krasovitski & Marmur 2005), which is a complicated problem in the case of the three-dimensional geometry. In the present work, we will assume that the CAH is equal to the term corresponding to the adhesion hysteresis ΔW plus the term corresponding to the effect of surface roughness, H_r. We also assume that equation (2.5), which normally applies to the thermodynamic equilibrium and is valid for the most stable CA, applies also to the effect of the adhesion hysteresis upon the CAH. Then, using equation (2.5), the CAH is related to the adhesion hysteresis as

$$\cos\theta_{a0} - \cos\theta_{r0} = \frac{\Delta W_0}{\gamma_{LA}} + H_r, \tag{2.6}$$

where θ_{a0} and θ_{r0} are the advancing and receding CA for a smooth surface, respectively, and ΔW_0 is the corresponding value of adhesion hysteresis. For a composite interface, adhesion hysteresis is proportional to the solid–liquid area

$$\Delta W = f_{SL} R_f \Delta W_0. \tag{2.7}$$

The CAH is obtained by combining equations (2.5)–(2.7)

$$\begin{aligned}\cos\theta_a - \cos\theta_r &= \frac{\Delta W}{\gamma_{LA}} = \frac{R_f f_{SL} \Delta W_0}{\gamma_{LA}} \\ &= R_f f_{SL}(\cos\theta_{a0} - \cos\theta_{r0}) + H_r,\end{aligned} \tag{2.8}$$

where θ_a and θ_r are the advancing and receding CA for a rough surface, respectively. For the homogeneous interface, $f_{SL} = 1$, whereas for composite interface, f_{SL} is a small number. It is observed from equation (2.8) that for a homogeneous interface, increasing roughness (high R_f) leads to the increased CAH (high values of $\theta_a - \theta_r$), while for a composite interface, small values of f_{SL} provide both high CA and low CAH. Therefore, a composite interface is essential for superhydrophobicity, which involves both high CA and low CAH.

For a droplet of radius R moving along the inclined plane with angle α (figure 1), the energy gain corresponding to the inclined distance l is given by $lmg \sin\alpha$, where mg is the weight of the droplet. Marmur (1994) and Krasovitski & Marmur (2005) showed that the droplet on an inclined plane does not necessarily exhibit the receding or advancing CA, since the former is based on the

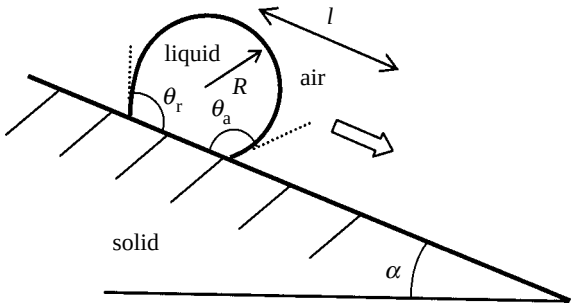

Figure 1. Schematics of a droplet moving along an inclined surface with TA α, advancing CA θ_a and receding CA θ_r.

geometry of the drop, whereas the latter is based on the nature of the solid surface. Therefore, we will use the energy balance method to determine the TA. The energy loss is given by ΔW times the contact area $lR\sin\theta$. Combining these equations with equation (2.7), the TA is given by

$$\sin\alpha = \frac{\Delta W_0 f_{SL} R_f R \sin\theta}{mg}. \tag{2.9}$$

Using the trigonometric relationship

$$\cos\theta_a - \cos\theta_r = -2\sin\frac{\theta_a+\theta_r}{2}\sin\frac{\theta_a-\theta_r}{2}, \tag{2.10}$$

and substituting into equation (2.8)

$$\sin\frac{\theta_a-\theta_r}{2} = -\frac{mg}{2R\gamma_{LA}\sin\theta\sin\frac{\theta_a+\theta_r}{2}}\sin\alpha. \tag{2.11}$$

For θ and $(\theta_a+\theta_r)/2$ close to π, it is found from equation (2.11) that the TA is proportional to the CAH.

For patterned surfaces, it is convenient to introduce a non-dimensional parameter, the spacing factor

$$S_f = \frac{D}{P}, \tag{2.12}$$

where D is the diameter of the pillars and P is the pitch distance between them. The main contribution of roughness is expected to be from the sharp edges of the pillars, which may pin a moving droplet (Nosonovsky & Bhushan 2005). Therefore, the surface roughness term is assumed to be proportional to the density of the edges, which is equal to the total perimeter of the pillars per unit area, $H_r \propto \pi D/P^2$ or

$$H_r = cS_f^2, \tag{2.13}$$

where c is a non-dimensional proportionality constant. Since, for the flat-top pillars, $R_f=1$ and

$$f_{SL} = \frac{\pi S_f^2}{4}, \tag{2.14}$$

the CA, CAH and TA can easily be presented as functions of S_f using equations (2.4), (2.8) and (2.9).

3. EXPERIMENTAL DETAILS

The static and dynamic CAs were measured using a Rame-Hart model 100 CA goniometer[1] and water droplets of deionized water. Droplets of 5 µl size (diameter of a spherical droplet is 2 mm) were gently deposited on the substrate using a microsyringe for the static CA. The receding CA was measured by the removal of water from a deionized water sessile drop (approx. 5 µl) using a microsyringe. The advancing CA was measured by adding additional water to the sessile drop (approx. 5 µl) using the microsyringe. The CAH was calculated by the difference between the measured advancing and receding CA. The TA was measured by a simple stage tilting experiment with the droplets of 5 µl size. All measurements were made by five different points for each sample at 22±1°C and 50±5% relative humidity. The measurements were reproducible to within ±3°. For surface roughness, an optical profiler (NT-3300, Wyko Corp., Tuscon, AZ) was used for different patterned surface structures (figure 2). A scan size of 100×90 µm was used to scan the patterned surface.

Single-crystal silicon (Si) was used in this study. Silicon material has traditionally been the most commonly used structural material for micro/nanocomponents (Bhushan 2007). A Si structure can be made hydrophobic by coating it with a self-assembled monolayer (SAM). For patterned Si, two series of nine samples each were fabricated using photolithography. Series 1 has 5 µm diameter and 10 µm height flat-top, cylindrical pillars with different pitch values (7, 7.5, 10, 12.5, 25, 37.5, 45, 60 and 75 µm), and Series 2 has 14 µm diameter and 30 µm height flat-top, cylindrical pillars with different pitch values (21, 23, 26, 35, 70, 105, 126, 168, and 210 µm). The Si chosen were initially hydrophilic, hence to obtain a sample that is hydrophobic, the SAM of 1,1,2,2-tetrahydroperfluorodecyltrichlorosilane (PF_3) was deposited on the sample surfaces using vapour-phase deposition technique (Bhushan *et al.* 2006; Barbieri 2006). PF_3 was chosen owing to the hydrophobic nature of the surface.

4. RESULTS AND DISCUSSION

An optical profiler was used to measure the surface topography of the patterned surfaces. One sample each from the two series was chosen to characterize the surfaces. Two different surface height maps can be seen for the patterned Si in figure 2. In each figure, a three-dimensional map and a flat map along with a two-dimensional profile in a given location of the flat three-dimensional map are shown. A scan size of 100×90 µm was used not only to obtain a sufficient amount of pillars to characterize the surface, but also to maintain enough resolution to get an accurate measurement. The images obtained with the optical profiler show the flat-top, cylindrical pillars on the Si surface distributed at the entire surface in a square grid with different pitch values, referred to as series 1 (5 µm in diameter and pillars of 10 µm in height) and series 2 (14 µm in diameter and pillars of 30 µm in height).

Results for the CA, CAH and TA of patterned Si coated with PF_3 are presented in figure 3 as a function of the spacing factor S_f measured in two series of the experiments, with flat-top, cylindrical pillars of diameters $D=5$ and 14 µm and heights $H=10$ and 30 µm, respectively. The flat Si coated with PF_3 showed static CA of 109°. As the spacing factor decreases down to $S_f=0.11$ (the pitch of 45 µm in series 1 and 126 µm in series 2), the static CA increases gradually from 152 to

[1]Certain instruments and materials are identified to adequately specify the experimental procedure. Such identification does not imply recommendation or endorsement by the National Institute of Standards and Technology, nor does it imply that the materials or instruments identified are necessarily the best available for the purpose.

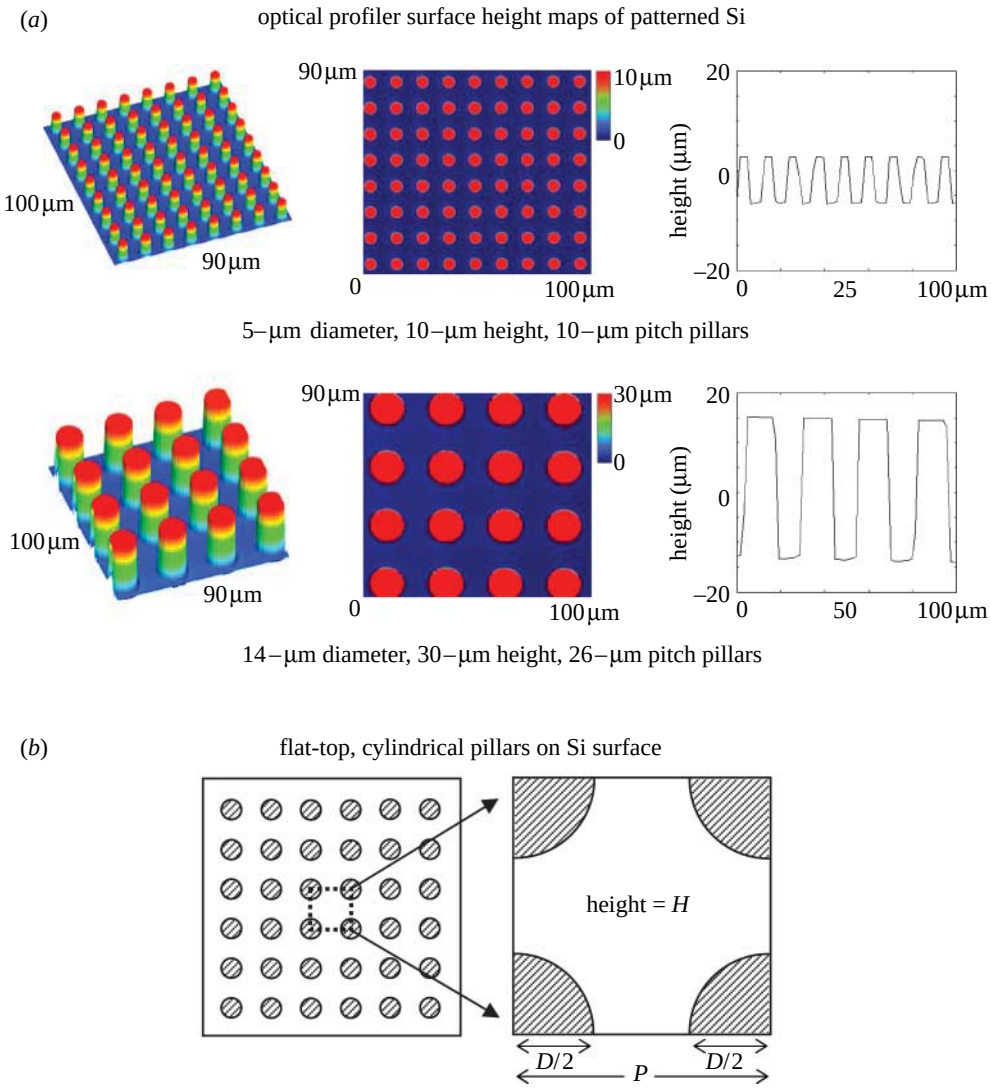

Figure 2. (*a*) Surface height maps and two-dimensional profile of the patterned Si surfaces using an optical profiler. (*b*) Two-dimensional representation of flat-top, cylindrical pillars on a patterned Si surfaces. The diameter and height of the pillar are D and H, respectively. The pitch between pillars is P.

170° (figure 3*a*). Then, the CA starts decreasing sharply, indicating a transition from the composite to homogeneous interface. It is noted that the transition takes place at the critical value of $0.083 < S_f < 0.111$ for both the series. Since droplets of the same size (5 µl) were used for both the series, this suggests that the spacing factor and the fractional solid–liquid area of contact (which is directly related to S_f according to equation (2.12)) are responsible for the transition, whereas the ratio of the pillar size to the size of the droplet does not matter. The values of the CA are plotted against the theoretically predicted value, based on the Wenzel (calculated using equation (2.2), $R_f = 1+\pi HD/P^2$) and Cassie–Baxter (calculated using equations (2.4) and (2.14)) models. There is a good agreement between the experimental data for the composite interface with the Cassie–Baxter model and for the homogeneous interface with the Wenzel model.

Figure 3*b* shows CAH and TA as functions of the spacing factor. The flat Si coated with PF_3 showed the advancing CA of 116°, the receding CA of 82°, CAH of 34° and TA of 37°. There is a good correlation between the CAH data and the TA in the case of small values of the CA, while for the large values of the CA, the correlation is worse. This is consistent with equation (2.11). CAH and TA show the same trends as CA with varying S_f. They gradually decrease with decreasing S_f and show an abrupt minimum in the value, which corresponds to the highest contact angle. The lowest hysteresis and TAs are 5° and 3°, respectively, which were observed at $S_f = 0.111$.

Figure 3*c* shows the theoretically predicted values of the CAH $\cos\theta_r - \cos\theta_a$ for the composite interface (calculated using equations (2.8), (2.13) and (2.14)) plotted against the experimentally measured values for $c = 0$, 0.25 and 0.5. There is a good agreement between the experimental data and the theoretically predicted values for $c = 0.5$. It is noted that the theoretically predicted values for $c = 0$ (no effect of the surface roughness) underestimate CAH, with the experimental values approximately twice larger. This result suggests that the contact area and the adhesion hysteresis give approximately the same contribution to the CAH as the roughness and sharp edges, while the calculation based upon equations (2.8) and (2.14) gives a good agreement with the experimental data for dynamic advancing and receding CA. Experimental observation shows that

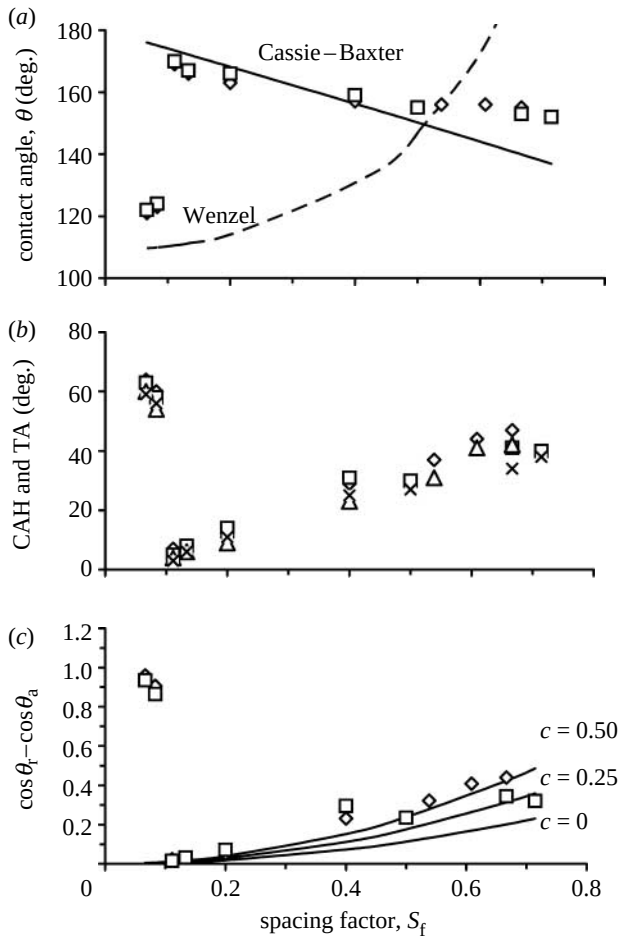

Figure 3. (*a*) Static CA θ as a function of the spacing factor S_f for the first (squares) and the second (diamonds) series of the experiments compared with the Wenzel (dashed line) and Cassie–Baxter (solid lines) models. (*b*) CAH (squares for the first series and diamonds for the second) and TA (crosses for the first series and triangles for the second) as a function of S_f. (*c*) The values of $\cos\theta_r - \cos\theta_a$ as a function of S_f for the first (squares) and the second (diamonds) series of the experiments compared with the theoretically predicted values for various values of c (solid line).

pinning of the droplet at the edges of the pillars indeed takes place during the motion of the droplet and thus pinning affects the CAH.

5. CONCLUSIONS

We have studied experimentally and theoretically the wetting of patterned Si surfaces with cylindrical flat-top pillars of various sizes and pitch distances between them, covered with a hydrophobic PF_3 coating. The values of the CA, CAH and TA were measured. In order to achieve high values of CA and low values of CAH and TA, a composite interface should form. However, the composite interface is not always stable, and it may irreversibly transform into the homogeneous interface, leading to much higher CAH and TA. Transition from the composite to the homogeneous interface was investigated. It was found that the transition occurs at a critical value of a non-dimensional parameter (the spacing factor) independent of the actual size of the roughness and its ratio to the droplet size. This result is different from the energy minimum criterion proposed earlier (Lafuma & Quéré 2003; Fürstner *et al.* 2005). The spacing factor is equal to the pillar diameter divided by the pitch. The CA is a function of the spacing factor for both the composite and the homogeneous interfaces and may be theoretically predicted with reasonable accuracy using the Cassie–Baxter and Wenzel models, respectively.

The values of the CAH were measured experimentally. The theoretical values of the CAH were calculated as a function of the spacing factor based on the assumption that the adhesion hysteresis between the solid and the liquid and pillar edges density are the main contribution to the CAH. The adhesion hysteresis is a difference of the work of adhesion at the separation of the solid and liquid surfaces and the energy gained at bringing them together. The pillar edges may result in the pinning of the droplet. The experimental values of the CAH show a good agreement with the theoretically calculated values. Similar to the CA, the CAH depends upon the non-dimensional spacing factor and was found independent of the actual size of roughness.

The TA was measured experimentally. The values of the TA correlate very well with the values of the CAH in the case of the composite interface. This result is predicted theoretically for small CAH, while the latter is calculated based on the above-mentioned assumption.

To summarize, we found that the wetting behaviour of a patterned hydrophobic surface is governed by a simple non-dimensional parameter, the spacing factor. The spacing factor controls the CA, CAH and TA in the desired composite interface regime, as well as destabilization and undesirable transition to the homogeneous interface. By decreasing the spacing factor to the value $S_f = 0.111$, the CA $\theta = 170°$, CAH $\theta_a - \theta_r = 5°$ and TA $\alpha = 3°$ values were achieved. However, with further decreasing of the spacing factor, the composite interface destabilizes and the values of CA abruptly decrease, while CAH and TA increase. We also found that the assumption that the CAH is a consequence of both the adhesion hysteresis and the surface roughness leads to the theoretical values of the CAH, which are in a reasonably good agreement with the experimental values.

Financial support for this project was provided in part by the National Science Foundation (no. ECS-0301056). The patterned samples were provided by Drs Patrik Hoffmann and Laura Barbieri of Ecole Polytechnique Federale de Lausanne Switzerland.

REFERENCES

Adamson, A. V. 1990 *Physical chemistry of surfaces*. New York, NY: Wiley.

Barbieri, L. 2006 Wetting properties of flat-top periodically structured superhydrophobic surfaces. Ph.D. thesis, EPFL, Lausanne, Switzerland.

Barthlott, W. & Neinhuis, C. 1997 Purity of the sacred lotus, or escape from contamination in biological surfaces. *Planta* **202**, 1–8. (doi:10.1007/s004250050096)

Bhushan, B. 1999 *Handbook of micro/nanotribology*, 2nd edn. Boca Raton, FL: CRC Press.

Bhushan, B. 2002 *Introduction to tribology*. New York, NY: Wiley.

Bhushan, B. 2005 *Nanotribology and nanomechanics—an introduction*. Heidelberg, Germany: Springer.

Bhushan, B. 2007 *Springer handbook of nanotechnology*, 2nd edn. Heidelberg, Germany: Springer.

Bhushan, B. & Jung, Y. C. 2006 Micro- and nanoscale characterization of hydrophobic and hydrophilic leaf surfaces. *Nanotechnology* **17**, 2758–2772. (doi:10.1088/0957-4484/17/11/008)

Bhushan, B., Hansford, D. & Lee, K. K. 2006 Surface modification of silicon and polydimethylsiloxane surfaces with vapor-phase-deposited ultrathin fluorosilane films for biomedical nanodevices. *J. Vac. Sci. Technol. A* **24**, 1197–1202. (doi:10.1116/1.2167077)

Bico, J., Thiele, U. & Quere, D. 2002 Wetting of textured surfaces. *Colloid. Surface. A* **206**, 41–46. (doi:10.1016/S0927-7757(02)00061-4)

Burton, Z. & Bhushan, B. 2005 Hydrophobicity, adhesion and friction properties of nanopatterned polymers and scale dependence for MEMS/NEMS. *Nano Lett.* **5**, 1607–1613. (doi:10.1021/nl050861b)

Burton, Z. & Bhushan, B. 2006 Surface characterization and adhesion and friction properties of hydrophobic leaf surfaces. *Ultramicroscopy* **106**, 709–716. (doi:10.1016/j.ultramic.2005.10.007)

Cassie, A. & Baxter, S. 1944 Wettability of porous surfaces. *Trans. Faraday Soc.* **40**, 546–551. (doi:10.1039/tf9444000546)

Chen, W., Fadeev, A. Y., Hsieh, M. C., Öner, D., Youngblood, J. & McCarthy, T. J. 1999 Ultrahydrophobic and ultralyophobic surfaces: some comments and examples. *Langmuir* **15**, 3395–3399. (doi:10.1021/la990074s)

Coulson, S. R., Woodward, I. & Badyal, J. P. S. 2000 Super-repellent composite fluoropolymer surfaces. *J. Phys. Chem. B* **104**, 8836–8840. (doi:10.1021/jp0000174)

Erbil, H. Y. 2003 Transformation of a simple plastic into a superhydrophobic surface. *Science* **299**, 1377–1380. (doi:10.1126/science.1078365)

Extrand, C. W. 2002 Model for contact angle and hysteresis on rough and ultraphobic surfaces. *Langmuir* **18**, 7991–7999. (doi:10.1021/la025769z)

Extrand, C. W. 2006 Designing for optimum liquid repellency. *Langmuir* **22**, 1711–1714. (doi:10.1021/la052540l)

Feng, L. *et al.* 2002 Super-hydrophobic surfaces: from natural to artificial. *Adv. Mater.* **14**, 1857–1860. (doi:10.1002/adma.200290020)

Fürstner, R., Barthlott, W., Neinhuis, C. & Walzel, P. 2005 Wetting and self-cleaning properties of artificial superhydrophobic surfaces. *Langmuir* **21**, 956–961. (doi:10.1021/la0401011)

Gao, L. & McCarthy, T. J. 2006 The lotus effect explained: two reasons why two length scales of topography are important. *Langmuir* **22**, 2966–2967. (doi:10.1021/la0532149)

He, B., Patankar, N. A. & Lee, J. 2003 Multiple equilibrium droplet shapes and design criterion for rough hydrophobic surfaces. *Langmuir* **19**, 4999–5003. (doi:10.1021/la0268348)

Hozumi, A. & Takai, O. 1998 Preparation of silicon oxide films having a water-repellent layer by multiple-step microwave plasma-enhanced chemical vapor deposition. *Thin Solid Film* **334**, 54–59. (doi:10.1016/S0040-6090(98)01116-X)

Israelachvili, J. N. 1992 *Intermolecular and surface forces*, 2nd edn. London, UK: Academic Press.

Jetter, R., Kunst, L. & Samuels, A. L. 2006 Composition of plant cuticular waxes. In *Biology of the plant cuticle* (eds M. Riederer & C. Müller), pp. 145–181. Oxford, UK: Blackwell Publishing.

Johnson, R. E. & Dettre, R. H. 1964 Contact angle hysteresis. In *Contact angle, wettability, and adhesion*, vol. 43 (ed. F. M. Fowkes) *Advances in chemistry series*, pp. 112–135. Washington, DC: American Chemical Society.

Jung, Y. C. & Bhushan, B. 2006 Contact angle, adhesion and friction properties of micro- and nanopatterned polymers for superhydrophobicity. *Nanotechnology* **17**, 4970–4980. (doi:10.1088/0957-4484/17/19/033)

Kijlstra, J., Reihs, K. & Klami, A. 2002 Roughness and topology of ultra-hydrophobic surfaces. *Colloid. Surface. A Physicochem. Eng. Aspects* **206**, 521–529. (doi:10.1016/S0927-7757(02)00089-4)

Krasovitski, B. & Marmur, A. 2005 Drops down the hill: theoretical study of limiting contact angles and the hysteresis range on a tilted plate. *Langmuir* **21**, 3881–3885. (doi:10.1021/la0474565)

Lafuma, A. & Quéré, D. 2003 Superhydrophobic states. *Nat. Mater.* **2**, 457–460. (doi:10.1038/nmat924)

Lau, K. K. S., Bico, J., Teo, K. B. K., Chhowalla, M., Amaratunga, G. A. J., Milne, W. L., Mckinley, G. H. & Gleason, K. K. 2003 Superhydrophobic carbon nanotube forests. *Nano Lett.* **3**, 1701–1705. (doi:10.1021/nl034704t)

Li, W. & Amirfazli, A. 2005 A thermodynamic approach for determining the contact angle hysteresis for superhydrophobic surfaces. *J. Colloid Interface Sci.* **292**, 195–201. (doi:10.1016/j.jcis.2005.05.062)

Marmur, A. 1994 Thermodynamic aspects of contact angle hysteresis. *Adv. Colloid Interface Sci.* **50**, 121–141. (doi:10.1016/0001-8686(94)80028-6)

Marmur, A. 2003 Wetting on hydrophobic rough surfaces: to be heterogeneous or not to be? *Langmuir* **19**, 8343–8348. (doi:10.1021/la0344682)

Miwa, M., Nakajima, A., Fujishima, A., Hashimoto, K. & Watanabe, T. 2000 Effects of the surface roughness on sliding angles of water droplets on superhydrophobic surfaces. *Langmuir* **16**, 5754–5760. (doi:10.1021/la991660o)

Neinhuis, C. & Barthlott, W. 1997 Characterization and distribution of water-repellent, self-cleaning plant surfaces. *Ann. Bot.* **79**, 667–677. (doi:10.1006/anbo.1997.0400)

Nosonovsky, M. & Bhushan, B. 2005 Roughness optimization for biomimetic superhydrophobic surfaces. *Microsyst. Technol.* **11**, 535–549. (doi:10.1007/s00542-005-0602-9)

Nosonovsky, M. & Bhushan, B. 2006 Stochastic model for metastable wetting of roughness-induced superhydrophobic surfaces. *Microsyst. Technol.* **12**, 273–281. (doi:10.1007/s00542-005-0067-x)

Nosonovsky M. & Bhushan B. In press. Hierarchical roughness makes superhydrophobic surfaces stable. *Microelectron. Eng.*

Oner, D. & McCarthy, T. J. 2000 Ultrahydrophobic surfaces. Effects of topography length scales on wettability. *Langmuir* **16**, 7777–7782. (doi:10.1021/la000598o)

Patankar, N. A. 2003 On the modeling of hydrophobic contact angles on rough surfaces. *Langmuir* **19**, 1249–1253. (doi:10.1021/la026612+)

Ruths, M., Berman, A. D. & Israelachvili, J. N. 2005 Surface forces and nanorheology of molecularly thin films. In *Nanotribology and Nanomechanics. An Introduction* (ed. B. Bhushan), pp. 389–482. Berlin, Germany: Springer.

Shibuichi, S., Onda, T., Satoh, N. & Tsujii, K. 1996 Super-water-repellent surfaces resulting from fractal structure. *J. Phys. Chem.* **100**, 19 512–19 517. (doi:10.1021/jp9616728)

Wagner, P., Furstner, F., Barthlott, W. & Neinhuis, C. 2003 Quantitative assessment to the structural basis of water repellency in natural and technical surfaces. *J. Exp. Bot.* **54**, 1295–1303. (doi:10.1093/jxb/erg127)

Wolansky, G. & Marmur, A. 1998 The actual contact angle on a heterogeneous rough surface in three dimensions. *Langmuir* **14**, 5292–5297. (doi:10.1021/la960723p)